Fuel 334 (2023) 126799

Contents lists available at ScienceDirect

Fuel

journal homepage: www.elsevier.com/locate/fuel

Full Length Article

Bimetallic Ru–Pd supported on CeO_2 for the catalytic partial oxidation of methane into syngas

Shiva Fazlikeshteli, Xavier Vendrell [*,1], Jordi Llorca [*]

Institute of Energy Technologies, Department of Chemical Engineering and Barcelona Research Center in Multiscale Science and Engineering, Universitat Politècnica de Catalunya, EEBE, Eduard Maristany 10–14, 08019 Barcelona, Spain

ARTICLE INFO

Keywords:
Partial oxidation of methane
Syngas
Bimetallic catalysts
Noble metal catalysts
Ceria catalysts
Mechanochemistry

ABSTRACT

A series of monometallic Ru, Pd, and bimetallic Ru–Pd catalysts loaded on CeO_2 support have been prepared via mechanochemical and conventional incipient wetness impregnation methods and used in the partial oxidation of methane (POM) to obtain synthesis gas (H_2 and CO). The influence of the preparation method, the order of addition of the metals, the Ru:Pd metal ratio, and the milling energy and time for samples prepared by the mechanochemical method, have been evaluated between 300 and 600 °C. The results revealed that bimetallic Ru–Pd/CeO_2 catalysts outperform monometallic Ru–CeO_2 and Pd–CeO_2 for POM, both in terms of catalytic activity and stability. Additionally, the bimetallic Ru–Pd/CeO_2 catalysts prepared by ball milling produced syngas at a much lower temperature compared to the conventional catalysts prepared by incipient wetness impregnation. Raman spectroscopy, temperature programmed reduction (H_2–TPR), X–ray photoelectron spectroscopy (XPS) and high–resolution transmission electron microscopy (HRTEM) have been used to characterize the catalysts before and after reaction.

1. Introduction

Synthesis gas (syngas), the mixture of H_2 and CO, is an important raw material widely used to produce hydrogen, alcohols, synthetic fuels, and other chemical products [1]. Nowadays, the most common industrial technologies to produce syngas are the steam reforming of methane (SRM) (Eq. (1)) [2], dry reforming of methane (DRM) (Eq. (2)) [3], partial oxidation of methane (POM) (Eq. (3)) [4], and oxidative reforming of methane (Eq. (4)) [5].

$$CH_4 + H_2O \rightarrow CO + 3H_2 \quad \Delta H^{\circ}_{298K} = 206\ kJ\ mol^{--1} \tag{1}$$

$$CH_4 + CO_2 \rightarrow 2H_2 + 2CO \quad \Delta H^{\circ}_{298K} = 247\ kJ\ mol^{--1} \tag{2}$$

$$CH_4 + \frac{1}{2}O_2 \rightarrow CO + 2H_2 \quad \Delta H^{\circ}_{298K} = --36kJ\ mol^{--1} \tag{3}$$

$$CH_4 + \frac{x}{2}O_2 + (1--x)H_2O \rightarrow CO + (3--x)H_2 \Delta H^{\circ}_{298K} = 206--242x\ kJ\ mol^{--1} \tag{4}$$

Compared with the former two, the POM process has distinct advantages, including (i) it is a mildly exothermic reaction and no external heat source is necessary to sustain the process, while the SRM and DRM are highly endothermic reactions, thus, the industrial process based upon POM is energy–saving [6], (ii) high conversion and selectivity at lower process temperature [7], (iii) the capability to produce syngas with a H_2/CO molar ratio of ~ 2, which is suitable for downstream processes such as methanol synthesis, Fischer–Tropsch, etc. [4], (iv) POM can be carried out under high gas hourly space velocity (GHSV), which means less investment and less production scale to achieve the same capacity [8]. Because of the above characteristics, POM represents the most economical technology for syngas production and has attracted special attention [9].

Generally, two kinds of catalyst formulations are primarily applied for the catalytic partial oxidation of methane to achieve high conversion of methane and high selectivity to syngas. These are: (i) supported noble metal–based catalysts (Rh, Ru, Ir, Pt and Pd) [10], and (ii) supported first–row transition metal–based catalysts (Ni, Co and Cu) [11]. Typical supports are Al_2O_3 [8] and CeO_2 [12]. Noble metals are widely used because, even if they are much more expensive, they are highly active

* Corresponding authors.
E-mail addresses: xavier.vendrell@ub.edu (X. Vendrell), jordi.llorca@upc.edu (J. Llorca).
[1] Current address: Inorganic & Organic Chemistry Department, Inorganic section, Institute of Nanoscience & Nanotechnology (IN2UB), Universitat de Barcelona, Martí i Franquès, 1, 08028, Barcelona, Spain.

https://doi.org/10.1016/j.fuel.2022.126799
Received 12 July 2022; Received in revised form 13 October 2022; Accepted 13 November 2022
Available online 21 November 2022
0016-2361/© 2022 The Author(s). Published by Elsevier Ltd. This is an open access article under the CC BY-NC-ND license (http://creativecommons.org/licenses/by-nc-nd/4.0/).

and less sensitive to coke formation [7]. Green and co–workers showed that for stoichiometric partial oxidation with air, high methane conversion (~94 %) and high syngas yield (H_2 ~ 99 %, CO ~ 97 %) can be obtained at 1050 K and 1 bar over nearly all the noble metal catalysts, as well as over rare earth ruthenium pyrochlores [13,14]. Hickman et al. [15–17] and Poirier et al. [18] studied POM over Rh and Pt–Pd catalysts. It was reported that these noble metal catalysts, even with very low metal loadings, were much more active than Ni catalysts. It was shown by Horn et al. [19] that CH_4 could be converted into syngas on Rh and Pt foam catalysts with high selectivity. Kunimori et al. [20,21] also found that Rh-based catalysts (VO_4/SiO_2 and Rh/SiO_2) are excellent catalysts for POM, even at 500 °C. Schmidt et al. [22] compared the activities of catalytic monoliths loaded with Rh, Pt, Ir, Pd, Pd, Ni, Fe, Co and Re and concluded that the best performance was achieved on Ru.

Bimetallic catalysts are attractive because the addition of the second metal modifies the structure and electronic properties of the monometallic catalyst [23,24], which may increase the catalytic activity, improve the selectivity and suppress catalytic deactivation [10]. The bimetallic catalysts might consist of two noble metals [25], non–noble and noble [26], as well as two non–noble metals [27]. The choice of a proper support has been found crucial in addressing the catalytic performance, selectivity, and thermal stability of catalysts for the POM process [28]. The use of a reducible support, such as cerium oxide (CeO_2), results in remarkably low–temperature POM activity. Cerium oxide is very effective as structural support and shows unique electronic properties [29,30]. Moreover, it is often utilized to promote catalytic activity and minimize coke formation in the POM process due to its high oxygen storage capacity [31–33]. The peculiar redox properties of CeO_2 involving the facile exchange between Ce^{3+} and Ce^{4+} states and the high mobility of O^{2-} ions in the lattice are the key factors to suppress carbon deposition [34].

In this paper, we focus on Ru–Pd bimetallic catalysts supported on CeO_2 to conduct the POM process at low temperature. In our previous work [35,37] we have observed the good performance of Pd–ceria–based catalysts for POM and the positive synergy between Pd and Ni (noble metal and non–noble–metal) for the reaction. Now we want to explore the Pd–Ru system as an example of noble metal–noble metal bimetallic formulation, taking into account the good performance of Ru–based catalysts for POM [22]. Therefore, we have prepared Ru–Pd/CeO_2 by two different methods, namely dry ball milling and conventional incipient wetness impregnation techniques. The ball milling technique has emerged recently as an important technological process for the preparation of catalysts because it is simple, fast, cost–effective, and environmentally–friendly. Importantly, the resulting materials have demonstrated enormous potential to activate C—H bonds for the transformation of methane [35–37]. We have also studied the importance of metal loading, metal ratios and order of incorporation of the metals and compared the results with monometallic Ru–CeO_2 and Pd–CeO_2.

2. Materials and methods

2.1. Preparation of CeO_2

Cerium nitrate hexahydrate ($Ce(NO_3)_3{\cdot}6H_2O$, 99.5 %) was purchased from Alfa Aesar and ammonia solution (NH_3, 28 %) was obtained from Scharlab. All reagents were used without further purification. CeO_2 was obtained by adding the ammonia solution dropwise to an aqueous solution of $Ce(NO_3)_3{\cdot}6H_2O$ until pH 9–10. The resulting product was filtered and thoroughly washed with deionized water. Finally, the precipitate was dried overnight at 90 °C and calcined in air at 650 °C for 4 h (5 °C min^{-1}).

2.2. Preparation of catalysts by mechanochemical method

Ruthenium (III) chloride ($RuCl_3$, 99.9 %) and palladium (II) nitrate ($Pd(NO_3)_2$, 93 %) were obtained from Acros Organics and used without further purification. Monometallic xRu–CeO_2/BM (x = 0.25 and 0.5 wt %) and yPd–CeO_2/BM (y = 0.5 and 1 wt%) catalysts were prepared by directly milling CeO_2 and the metal precursor in a zirconium oxide vessel using a Fritsch Pulverisette 23 mini–mill apparatus and one zirconium oxide ball of 15 mm diameter (ball to powder ratio, BPR = 10.2). These samples are labeled as BM. Two different routes were used to prepare the bimetallic xRu–yPd/CeO_2/BM catalysts (x = 0.06–1 wt%, y = 0.5–1.44 wt%, x + y = 1.5): (i) co–BM and (ii) sequential–BM. In the co–BM method, the bimetallic Ru–Pd catalysts were prepared in one step by milling together the two metal precursors with CeO_2. These catalysts were labeled as Ru–Pd/CeO_2/BM. In the sequential–BM method, firstly, one of the metal precursors was milled with CeO_2, and in a second step, the resulting material was milled with the other metal precursor. These samples were labeled as Ru–CeO_2/BM/Pd/BM or Pd–CeO_2/BM/Ru/BM depending if CeO_2 was first milled with the Ru precursor or with the Pd precursor, respectively. The effect of ball mill energy (15, 30 and 50 Hz) and milling time (5, 10 and 20 min) was investigated. All the fresh catalysts were used without any further treatment. The chemical composition of the catalysts determined by inductively-coupled plasma atomic emission spectroscopy (ICP-AES) showed that the metal loadings were virtually identical to the nominal values.

2.3. Preparation of catalysts by incipient wetness impregnation

Monometallic Ru/CeO_2 and Pd/CeO_2 as well as bimetallic Ru–Pd/CeO_2 catalysts were also prepared by conventional incipient wetness impregnation for comparison (labeled as IWI). For the preparation of monometallic xRu–CeO_2/IWI (x = 0.25 and 0. 5 wt%) and yPd–CeO_2/IWI (y = 0.5 and 1 wt%), an ethanol solution of $RuCl_3$ or $Pd(NO_3)_2$ was added slowly to the CeO_2 support. The samples were dried at 90 °C and calcined at 650 °C for 4 h (5 °C min^{-1}). Similarly, to the BM method, two different routes were used to prepare the bimetallic xRu–yPd/CeO_2/IWI catalysts (x = 0.06–1 wt%, y = 0.5–1.44 wt%, x + y = 1.5): (i) co–IWI and (ii) sequential–IWI. In the co–IWI, the Ru–Pd/CeO_2/IWI catalysts were prepared in one step by impregnating an ethanol solution containing both Ru and Pd precursors. These samples were labeled as Ru–Pd/CeO_2/IWI. In the sequential–IWI method, two consecutive incipient wetness impregnations were carried out, with a calcination step at 650 °C for 2 h after each impregnation. These samples were labeled as Ru–CeO_2/IWI/Pd/IWI or Pd–CeO_2/IWI/Ru/IWI depending if the first impregnation was carried out with the Ru or the Pd precursor, respectively. No further treatments were performed on the calcined samples before the catalytic test.

2.4. Catalytic tests

To study the catalytic performance for the POM process to syngas, a continuous–flow fixed–bed quartz reactor was used. Reactions were carried out at atmospheric pressure between 300 and 600 °C using a CH_4:air:N_2 mixture of 4:11:85 (CH_4/O_2 = 1.73) and F/W = 60 L h^{-1} g^{-1} (*g* refers to grams of catalyst), corresponding to a gas hourly space velocity of GHSV = 12 × $10^3 h^{-1}$). Typically, 0.1 g of the catalyst was mixed with SiC to obtain a fixed bed volume of 0.5 cm^3 in the reactor, and placed in the center of the heated zone of the furnace controlled with a proportional–integral–derivative (PID) temperature controller. The reaction products were analyzed online every 4 min with a Varian CP–4900 gas chromatograph equipped with a Molecular Sieve of 5 Å, Plot U, and Stabilwax columns. The methane conversion (X_{CH4}) (Eq. (5)), selectivity of hydrogen (S_{H2}) (Eq. (6)), selectivity of carbon monoxide (S_{CO}) (Eq. (7)), selectivity of carbon dioxide (S_{CO_2}) (Eq. (8)), and yield of syngas (Y_{sg}) (Eq. (9)) were evaluated from 300 °C to 600 °C at steps of 50 °C and calculated according to the following equations:

$$x_{CH4}(\%) = \frac{F_{inCH_4} - F_{outCH_4}}{F_{inCH_4}} \times 100 \quad (5)$$

where F_{inCH_4} and F_{outCH_4} are the inlet and outlet molar flow of methane, respectively.

$$S_{H2}(\%) = \frac{\dot{m}ofH_2produced}{\dot{m}of(H_2 + CO + CO_2)produced} \times 100 \quad (6)$$

$$S_{CO}(\%) = \frac{\dot{m}ofCOproduced}{\dot{m}of(H_2 + CO + CO_2)produced} \times 100 \quad (7)$$

$$S_{CO2}(\%) = \frac{\dot{m}ofCO_2produced}{\dot{m}of(H_2 + CO + CO_2)produced} \times 100 \quad (8)$$

$$Y_{sg}(\%) = \frac{x_{CH4} \times (S_{H2} + S_{CO})}{100} \quad (9)$$

Thermodynamic equilibrium compositions were calculated using the Bioanalytical Microfluidics Program [38].

2.5. Catalyst characterization

Raman spectroscopy was performed using a Renishaw inViaQontor confocal Raman microscope equipped with a 532.1 ± 0.3 nm laser with a nominal 100 mW output power directed through a specially adapted Leica DM2700 M microscope (x50 magnification). Thermo-gravimetric analysis (TGA) of the dried samples were conducted in air (40 mL min^{-1}) using a Q50 TA-instruments equipment from room temperature to 900 °C with a heating rate of 10 °C/min. Spectra were acquired in two ranges, 50–1200 cm^{-1} and 1200–2000 cm^{-1}, with an exposure time of 0.5 s, 1 % of maximum laser power, and 18 repetitions. H_2–temperature programmed reduction (H_2–TPR) was carried out with a Chemstar apparatus with a TCD detector. About 50 mg of sample was exposed to 50 mL min^{-1} of H_2 diluted in Ar (5 % H_2) from room temperature up to 850 °C (10 °C min^{-1}). The surface of the catalysts was analyzed by X–ray Photoelectron Spectroscopy (XPS) using a SPECS system equipped with an XR50 source operating at 250 W and a Phoibos 150 MCD–9 detector. The pass energy of the high–resolution spectra was set at 0.1 eV. Binding energy (BE) values were referred to the Ce^{4+} $3d_{5/2}$ peak at 916.9 eV. CasaXPS program (Casa Software ltd., UK) was used to evaluate the XPS data (Shirley type background). The chemical composition of the catalysts was determined by inductively-coupled plasma atomic emission spectroscopy (ICP-AES) using Perkin Elmer Optima 3200RL apparatus. The microstructure of the catalysts after the catalytic tests was investigated by high–resolution transmission electron microscopy (HRTEM) using a FEI TECNAI F20 instrument equipped with a field–emission electron source operated at 200 kV.

3. Results and discussion

3.1. Characterization of fresh catalysts

3.1.1. Raman spectroscopy

The Raman spectra recorded for fresh monometallic Ru, Pd, and bimetallic Ru–Pd catalysts supported on CeO_2 prepared by BM and IWI methods are shown in Fig. 1. For each sample, various spectra were recorded at several points and no differences were noted, indicating homogeneity of the samples. The Raman spectra were dominated by the characteristic F_{2g} band of the ceria lattice structure at about ~ 460 cm^{-1} [39]. The defect–induced vibrational mode at about ~ 595 cm^{-1} (D band) of ceria lattice defects, such as oxygen vacancies, was nearly absent in all samples, which indicates that the incorporation of Pd and Ru did not result in the formation of lattice defects in the ceria structure [40]. The Raman spectra of the monometallic 1Pd–CeO_2 catalysts prepared by IWI and BM methods and bimetallic 0.5Ru–CeO_2/IWI/1Pd–IWI catalyst exhibited a band at ~ 650 cm^{-1}, which is ascribed to the B_{1g} mode of PdO and suggests that these samples contain well–defined PdO nanoparticles [41]. Additionally, for the catalysts containing Pd and prepared by mechanochemistry (1Pd–CeO_2/BM and 0.5Ru–CeO_2/BM/1Pd/BM), a weak band at ~ 1050 cm^{-1} corresponding to the symmetric ν_1 stretching mode of the nitrate anion was observed [42]. The NO_3^- band was absent in the catalysts prepared by the IWI method because nitrate residues disappeared following the calcination treatment performed at 650 °C. Moreover, for the monometallic 0.5Ru–CeO_2 catalyst prepared by IWI method, a broadband at about 645–700 cm^{-1} is observed which it was attributed to the B_{2g} mode of RuO_2 [43]. No bands attributable to the Ru chloride precursor used were observed.

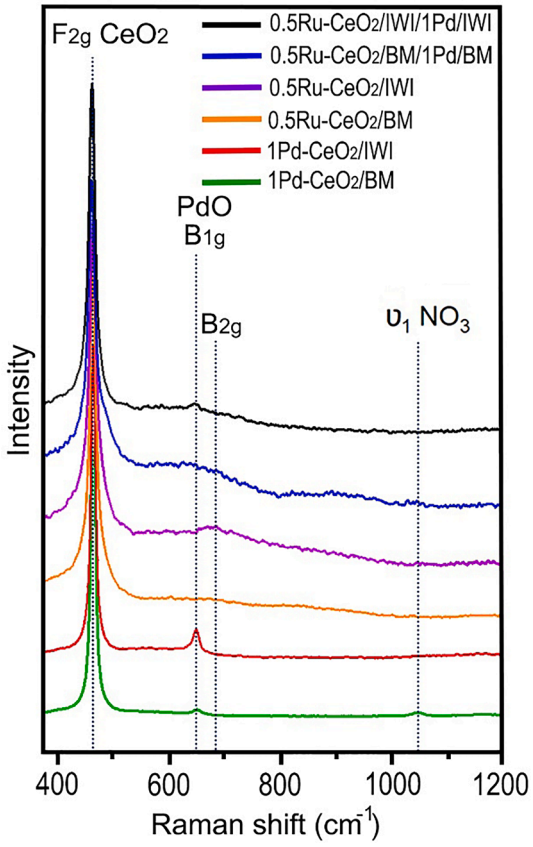

Fig. 1. Raman spectra of 1Pd–CeO_2 and 0.5Ru–CeO_2 samples prepared by BM and IWI methods, and bimetallic catalysts 0.5Ru–CeO_2/BM/1Pd/BM and 0.5Ru–CeO_2/IWI/1Pd/IWI. Ball milling conditions: 30 Hz and 10 min.

3.1.2. Temperature–programmed reduction (H_2–TPR)

H_2–TPR profiles are shown in Fig. 2. The profile of the CeO_2 support presented two peaks at around 530 °C and 780 °C, corresponding to the surface reduction of ceria involving bridging OH^- group formation, and the reduction of bulk Ce(IV) to Ce(III), respectively [43]{Watanabe, 2009 #97}{Lucentini, 2021 #95}. The bulk reduction peak of CeO_2 was detected in all the other samples analyzed, and it is quite clear, compared with monometallic Pd–CeO_2 catalysts prepared by both BM and IWI methods, that the bulk CeO_2 reduction peak for the bimetallic Ru–Pd catalysts are shifted to lower temperatures, which reveals that the simultaneous presence of Ru and Pd exerts a positive influence on the CeO_2 reduction.

The reduction profile of the monometallic Pd–CeO_2 catalyst prepared by BM exhibits two H_2 consumption peaks at about 150 and 293 °C. The reduction peak at ~ 150 °C is attributable to the reduction of surface PdO [44], while the intense consumption at ~ 293 °C can be assigned to the reduction of PdO–CeO_2 species strongly interacting with each other [45]. In contrast, the monometallic Pd–CeO_2 catalyst prepared by IWI did not show significant hydrogen consumption at low temperature. This represents a remarkable difference between the two Pd–CeO_2 catalyst and indicates that mechanochemistry originates a catalyst

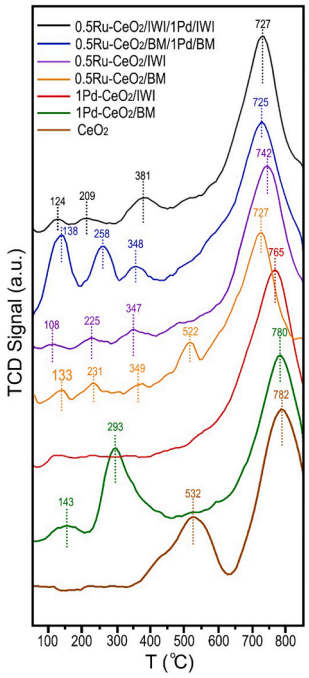

Fig. 2. H_2–TPR results of CeO_2, 1Pd–CeO_2 and 0.5Ru–CeO_2 samples prepared by BM and IWI methods, and bimetallic catalysts 0.5Ru–CeO_2/BM/1Pd/BM and 0.5Ru–CeO_2/IWI/1Pd/IWI. Ball milling conditions: 30 Hz and 10 min.

containing a strong interaction between Pd and CeO_2 [36]. Three reduction peaks were observed for the monometallic Ru–CeO_2 and bimetallic Ru–Pd/CeO_2 catalysts prepared by both IWI and BM methods in the range of 100–380 °C. According to literature data, the reduction peaks between 100 and 150 °C correspond to the reduction of RuO_x–type oxides (e.g. Ru_2O_3) different from RuO_2 [46], while the peaks at 210–380 °C are assigned to the reduction of well–dispersed ruthenium oxide particles on the surface of the ceria support [47]. Interestingly, the hydrogen consumption for the bimetallic Ru–Pd/CeO_2 catalyst prepared by ball milling is much higher than that of the bimetallic sample prepared by incipient wetness impregnation, particularly at low temperatures. This again points out to a particular, strong interaction between Pd and Ru and between the metals and the ceria support.

3.1.3. *X–ray photoelectron spectroscopy (XPS)*

The surface atomic composition of monometallic 1Pd–CeO_2, prepared by BM and IWI methods, and bimetallic 0.5Ru–CeO_2/BM/1Pd/BM and 0.5Ru–CeO_2/IWI/1Pd/IWI catalysts were analyzed by X-ray photoelectron spectroscopy (XPS) as shown in Fig. 3. Because of the low amount of ruthenium (≤0.5 wt%), Ru could not be identified on the surface of the bimetallic catalysts. Fig. 3(a) shows Ce 3d XPS of all the samples. No significant changes are observed in the Ce 3d spectra for all the catalysts. Additionally, the fitted components labeled V and U demonstrate the spin–orbit coupling $3d_{5/2}$ and $3d_{3/2}$, respectively. Three doublets were ascribed to the presence of Ce^{+4} labeled via: v (882.7 ~ eV), v_2 (889 ~ eV), v_3 (898.3 ~ eV), u (900.9 ~ eV), u_2 (907.6 ~ eV), and u_3 (916.9 ~ eV) [48]. A doublet v_0 (880.5 ~ eV), v_1 (885.6 ~ eV), u_0 (889.2 ~ eV), and u_1 (903.8 ~ eV) corresponding to the presence of Ce^{3+}, show a weak intensity due to the low proportion of Ce^{3+} [48]. Additionally, the analysis of the Ce 3d XPS revealed that for all monometallic and bimetallic catalysts the percentage of Ce^{4+} species calculated as $Ce^{4+}/(Ce^{4+}+ Ce^{3+})$ is ≥ 78 %.

On the other side, the Pd 3d core level XPS spectra for all samples were composed of two main doublets (Fig. 3b), confirming the presence of two types of Pd species on the surface [49]. The Pd $3d_{5/2}$ spectra contain two bands at about 336.3 and 337.9 eV, which correspond to

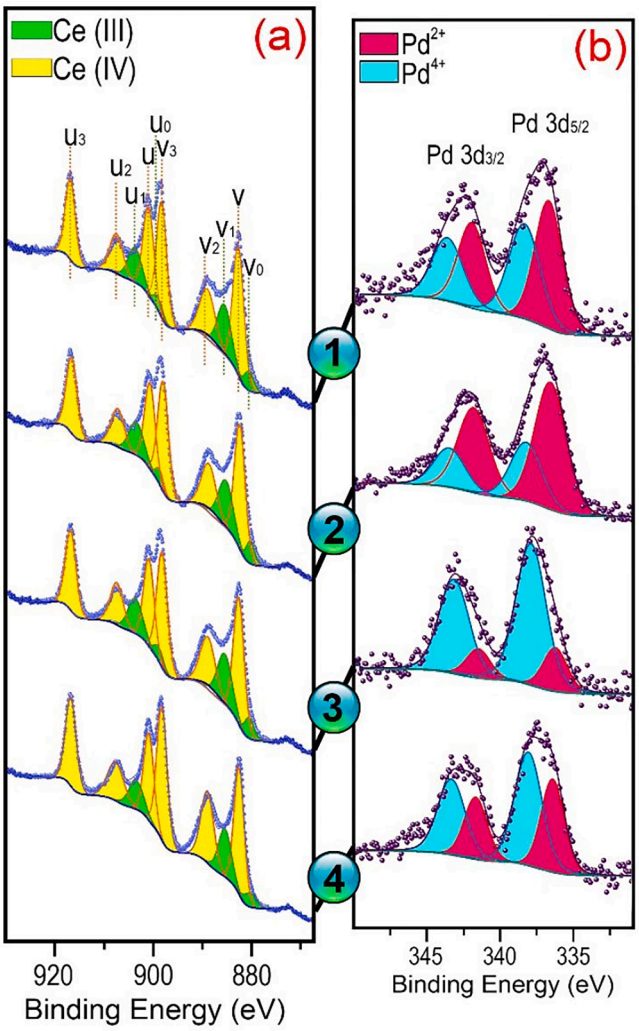

Fig. 3. Ce 3d (a) and Pd 3d (b) X–ray photoelectron spectra of monometallic 1Pd–CeO_2 catalysts prepared by BM (1) and IWI (2) methods, and bimetallic 0.5Ru–CeO_2/BM/1Pd/BM (3) and 0.5Ru–CeO_2/IWI/1Pd/IWI (4) catalysts. Ball milling conditions: 30 Hz and 10 min.

Pd^{2+} and Pd-O-Ce species, respectively [49]. Similarly, the Pd $3d_{3/2}$ spectra contain two bands related to Pd^{2+} (~341.5 eV) and Pd-O-Ce (~343.2 eV) species [35]. More interestingly, the Pd 3d core level XPS spectra show significant differences between the monometallic and bimetallic catalysts, where the intensity of Pd-O-Ce species in the bimetallic Ru–Pd/CeO_2 catalysts is greater when compared to monometallic Pd–CeO_2 catalysts, independently of the preparation method. The surface atomic ratio calculated as Pd-O-Ce/(Pd-O-Ce + Pd^{2+}) for these samples are: 1Pd–CeO_2/BM (0.63), 1Pd–CeO_2/IWI (0.49), 0.5Ru–CeO_2/BM/1Pd/BM (0.89), and 0.5Ru–CeO_2/IWI/1Pd/IWI (0.75). Therefore, it is concluded that Pd species strongly interacting with ceria (Pd-O-Ce) are easily accommodated on the surface of bimetallic Ru–Pd/CeO_2 catalysts.

3.2. *Catalytic tests*

Fig. 4 shows the molar flow rates of reactants (methane and oxygen) and products (hydrogen, carbon monoxide, water, and carbon dioxide) from 300 to 600 °C recorded on monometallic Ru, Pd, and bimetallic Ru–Pd catalysts supported on CeO_2 prepared by BM and IWI methods. According to thermodynamics, all samples followed similar trends in the disappearance of the reactants (CH_4 and O_2) and the appearance of the products (H_2 and CO). As expected, CH_4 conversion increased with

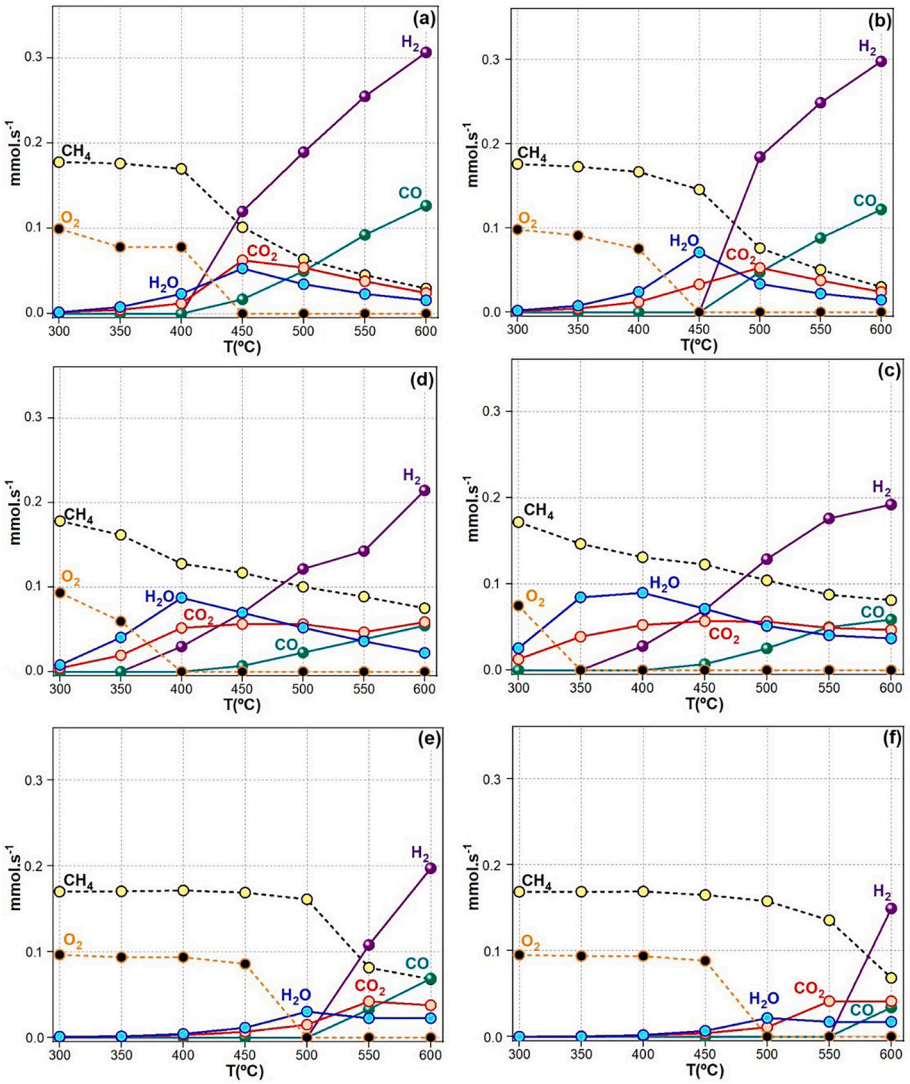

Fig. 4. Molar flows of bimetallic catalysts 0.5Ru–CeO_2/BM/1Pd/BM (a), 0.5Ru–CeO_2/IWI/1Pd/IWI (b), and monometallic catalysts 1Pd–CeO_2/BM (c), 1Pd–CeO_2/IWI (d), 0.5Ru–CeO_2/BM (e) and 0.5Ru–CeO_2/IWI (f). GHSV = 12 × $10^3 h^{-1}$, F/W = 60 L h^{-1} g^{-1}. Ball milling conditions: 30 Hz and 10 min.

increasing reaction temperature. In all cases, the distribution of intermediates and products is in accordance with the well–known combustion and reforming reaction (CRR) mechanism, where methane is first partially oxidized to yield H_2O and CO_2 and, as the temperature increases, the unreacted methane combines with H_2O and CO_2 to yield H_2 and CO through the steam reforming and dry reforming reactions (Eqs. (1) and (2), respectively) [50,51]. However, there is a significant difference between the Ru and Pd monometallic samples and the Ru–Pd bimetallic catalysts. Clearly, the bimetallic Ru–Pd catalysts exhibited higher catalytic activity and better syngas selectivity compared to monometallic Ru and Pd samples under the same operation conditions, pointing out to a beneficial effect of the synergy between the two metals. On the other hand, it should be noted that for all samples prepared by the IWI method the production of syngas occurred at higher temperature with respect to the samples prepared by the BM method. Considering the H_2–TPR and XPS results discussed above, it can be concluded that the strong interaction between Pd, Ru and CeO_2 that takes place in the catalysts prepared by ball milling with respect to those prepared by the conventional IWI method is responsible for a better catalytic performance.

Taking account these results, we prepared a series of monometallic and bimetallic catalysts varying the metal loading, the Pd:Ru elemental ratio, the order of incorporation of metals and, for those samples prepared by mechanochemistry, the milling conditions (frequency and time). Tables 1, 2 and 3 compile the catalytic results for all of them at 450–600 °C in terms of methane conversion (x_{CH4}), H_2 selectivity (S_{H2}), CO selectivity (S_{CO}), and yield of syngas (Y_{sg}). Chemical equilibrium values and catalytic results of milled CeO_2 are also included.

From Table 1, the CeO_2 support in the absence of Ru and Pd is inactive for the POM process under the reaction conditions tested. Moreover, it is clear that the catalytic activity of Pd–CeO_2 is higher than that of Ru–CeO_2 at temperatures $\leq$ 500 °C, as the CH_4 conversion values for Pd–CeO_2 catalysts with 0.5 wt% Pd prepared either by IWI or BM methods at 450 °C are ~ 30 % higher than those of the monometallic 0.5Ru–CeO_2 catalysts. It merits to be highlighted that the cooperative effect between Ru and Pd in the bimetallic catalysts is remarkable, with a dramatic increase in both the CH_4 conversion and the syngas yield compared to monometallic catalysts. At 600 °C, the bimetallic Ru–Pd/CeO_2 catalysts prepared by BM show CH_4 conversion levels from 79 to 85 % with a hydrogen selectivity of 66–67 %, CO selectivity of 26–28 %, and syngas yield between 71 and 80 %, very close to the values corresponding to the thermodynamic equilibrium. Additionally, the bimetallic Ru–Pd/CeO_2 catalysts prepared by the IWI method show methane conversion levels from 54 to 85 %, selectivity towards H_2 of 66–68 %, selectivity towards CO of 19–28 %, and syngas yield between 50 and 79 %. These values are clearly higher than those of the Pd/CeO_2 and Ru/

Table 1
Methane conversion, hydrogen, carbon monoxide, and carbon dioxide selectivity values, and syngas yield obtained over milled CeO_2, monometallic Ru–CeO_2 and Pd–CeO_2 samples prepared by ball milling (BM) and incipient wetness impregnation (IWI). Metal loading values are nominal. Reaction conditions: CH_4:air:N_2 = 4:11:85, F/W = 60 L h^{-1} g^{-1}, GHSV = 12 × 10^3h^{-1}.

Catalyst	Hz	min	wt.% Pd	wt.% Ru	$X_{CH_4}^{450^\circ C}$	$X_{CH_4}^{550^\circ C}$	$X_{CH_4}^{600^\circ C}$	$S_{H_2}^{600^\circ}$	$S_{CO}^{600^\circ C}$	$S_{CO_2}^{600^\circ C}$	$Y_{Syngas}^{600^\circ C}$
Equilibrium	–	–	–	–	51.3	77.9	89.4	65.4	30	4.5	85.3
CeO_2/BM	50	10	0	0	0	0	0	0	0	100	0
Ru–CeO_2/BM	30	10	0	0.25	5.4	38.5	52.1	62.0	17.1	20.9	41.2
Ru–CeO_2/IWI	–	–	0	0.25	1.9	7.8	41.8	65.8	9.5	24.7	31.5
Ru–CeO_2/BM	30	10	0	0.5	5.6	54.5	62	65.0	22.6	12.4	54.3
Ru–CeO_2/IWI	–	–	0	0.5	7.8	24.3	61.8	66.5	15.1	18.4	50.5
Ru–CeO_2/BM	30	10	0	1	10.9	62	71.8	66.3	20	13.8	61.9
Ru–CeO_2/IWI	–	–	0	1	16.3	60.4	74.1	65.1	21.7	13.2	64.3
Pd–CeO_2/BM	30	10	0.5	0	32.6	52.7	51.6	62.9	17.9	19.2	41.7
Pd–CeO_2/IWI	–	–	0.5	0	39.7	51.0	55.2	64.8	23.9	11.3	49.0
Pd–CeO_2/BM	30	10	1	0	31.5	51.0	54.6	64.6	19.7	15.7	46.0
Pd–CeO_2/IWI	–	–	1	0	34.5	50.3	58.0	65.4	16.6	17.9	47.6
Pd–CeO_2/BM	30	10	2	0	39.9	66.8	68.2	64.3	24.2	11.5	60.2
Pd–CeO_2/IWI	–	–	2	0	32.8	56	64.2	64.6	23.3	12.1	56.4

Table 2
Methane conversion, hydrogen, carbon monoxide, and carbon dioxide selectivity values, and syngas yield obtained over bimetallic Ru–Pd/CeO_2 catalysts prepared by ball milling (BM). Metal loading values are nominal. Reaction conditions: CH_4:air:N_2 = 4:11:85, F/W = 60 L h^{-1} g^{-1}, GHSV = 12 × 10^3h^{-1}.

Catalyst	Hz	min	wt.% Pd	wt.% Ru	$X_{CH_4}^{450^\circ C}$	$X_{CH_4}^{550^\circ C}$	$X_{CH_4}^{600^\circ}$	$S_{H_2}^{600^\circ C}$	$S_{CO}^{600^\circ C}$	$S_{CO_2}^{600^\circ C}$	$Y_{Syngas}^{600^\circ C}$
Equilibrium	–	–	–	–	51.3	77.9	89.4	65.4	30	4.5	85.3
Ru–Pd/CeO_2/BM	50	10	1	0.5	4.9	72.6	83.2	66.5	26.7	6.8	77.5
Pd–CeO_2/BM/Ru/BM	50	10	1	0.5	10.3	74.1	83.1	66.5	27.0	6.4	77.8
Ru–CeO_2/BM/Pd/BM	50	10	1	0.5	38.6	74.5	84.4	66.6	27.1	6.3	79.0
Ru–CeO_2/BM/Pd/BM	15	10	1	0.5	38.7	69.7	79.3	66.5	26.8	6.8	73.9
Ru–CeO_2/BM/Pd/BM	30	10	1	0.5	43.3	74.7	83.5	67.0	27.7	5.3	79.1
Ru–CeO_2/BM/Pd/BM	30	5	1	0.5	39.9	70.6	82.6	66.8	28.0	5.2	78.3
Ru–CeO_2/BM/Pd/BM	30	20	1	0.5	38.8	69.6	81.0	66.7	27.2	6.1	76.1
Ru–CeO_2/BM/Pd/BM	30	10	0.5	1	42.5	71.8	82.6	66.9	27.5	5.6	78.0
Ru–CeO_2/BM/Pd/BM	30	10	0.75	0.75	41.8	72.0	81.8	66.9	27.4	5.7	77.2
Ru–CeO_2/BM/Pd/BM	30	10	1.25	0.25	46.7	72.7	81.6	66.6	24.9	8.6	74.6
Ru–CeO_2/BM/Pd/BM	30	10	1.38	0.12	41.8	67.2	81.6	66.7	27.0	6.2	76.5
Ru–CeO_2/BM/Pd/BM	30	10	1.44	0.06	41.7	65.3	78.7	66.4	26.1	7.6	72.7

Table 3
Methane conversion, hydrogen, carbon monoxide, and carbon dioxide selectivity values, and syngas yield obtained over bimetallic Ru–Pd/CeO_2 catalysts prepared incipient wetness impregnation (IWI). Metal loading values are nominal. Reaction conditions: CH_4:air:N_2 = 4:11:85, F/W = 60 L h^{-1} g^{-1}, GHSV = 12 × 10^3h^{-1}.

Catalyst	Hz	min	wt.% Pd	wt.% Ru	$X_{CH_4}^{450^\circ C}$	$X_{CH_4}^{550^\circ C}$	$X_{CH_4}^{600^\circ}$	$S_{H_2}^{600^\circ C}$	$S_{CO}^{600^\circ C}$	$S_{CO_2}^{600^\circ C}$	$Y_{Syngas}^{600^\circ C}$
Equilibrium	–	–	–	–	51.3	77.9	89.4	65.4	30	4.5	85.3
Ru–Pd/CeO_2/IWI	–	–	1	0.5	2.7	72.7	82.0	66.7	27.1	6.1	77.0
Pd–CeO_2/IWI/Ru/IWI	–	–	1	0.5	4.8	72.9	84.3	67.2	27.7	5.1	80.0
Ru–CeO_2/IWI/Pd/IWI	–	–	1	0.5	18.5	71.8	83.2	67.1	27.5	5.4	78.7
Ru–CeO_2/IWI/Pd/IWI	–	—	0.5	1	43.2	73.5	83.4	68.2	23.0	8.9	76.0
Ru–CeO_2/IWI/Pd/IWI	–	–	0.75	0.75	42.8	71.4	82.9	67.3	25.8	7	77.2
Ru–CeO_2/IWI/Pd/IWI	–	–	1.25	0.25	23.0	66.5	67.7	66.0	19.0	14.9	57.7
Ru–CeO_2/IWI/Pd/IWI	–	–	1.38	0.12	16.5	55.4	68.9	65.6	21.7	12.7	60.1
Ru–CeO_2/IWI/Pd/IWI			1.44	0.06	17.1	54.0	54.2	66.7	26.0	7.3	50.1

CeO_2 catalysts (Table 1) and demonstrate that the synergy between Ru and Pd on CeO_2 yields catalysts with improved activity and selectivity for the POM with respect to the monometallic counterparts.

Fig. 5 illustrates the influence of the catalyst preparation method (co–impregnation or one–step ball milling vs sequential impregnation or two-step ball milling) and the milling conditions (frequency and time) for those catalysts prepared by mechanochemistry.

Fig. 5a shows the methane conversion at different temperatures (450 to 600 °C) for the bimetallic 0.5Ru–1Pd/CeO_2 catalysts prepared by co–impregnation (0.5Ru–1Pd/CeO_2/IWI) and by sequential impregnation by either impregnating first Pd or then Ru (1Pd–CeO_2/IWI/0.5Ru/IWI), or first Ru and then Pd (0.5Ru–CeO_2/IWI/1Pd/IWI). It is remarkable that the catalyst 0.5Ru–CeO_2/IWI/1Pd/IWI prepared by sequential impregnation (impregnating first Ru and then Pd) exhibits much higher catalytic activity at 450–500 °C than the catalysts prepared by co–impregnation or the catalyst prepared by sequential impregnation when Pd is impregnated first on CeO_2. In contrast, at higher reaction temperature, 550–600 °C, all IWI catalysts show a similar activity regardless of the order of metal addition. In a similar way, the bimetallic 0.5Ru–1Pd/CeO_2 catalyst prepared by two steps of ball milling adding first Ru (0.5Ru–CeO_2/BM/1Pd/BM) shows a remarkable higher catalytic activity at low temperature (Fig. 5b, 450 °C) than those of the catalyst prepared in one–step (0.5Ru–1Pd/CeO_2/BM) and two steps adding Pd first (1Pd–CeO_2/BM/0.5Ru/BM), whereas at higher reaction temperature (550–600 °C) similar methane conversion values are recorded regardless of the order of metal addition. This suggests that the effect of mechanical forces between the three components of the catalyst (ceria, Pd and Ru) originates a particular catalytic architecture which is extremely active at low temperature. The methane conversion values shown in Fig. 5a and 5b confirm, in all cases, that the catalytic activity of

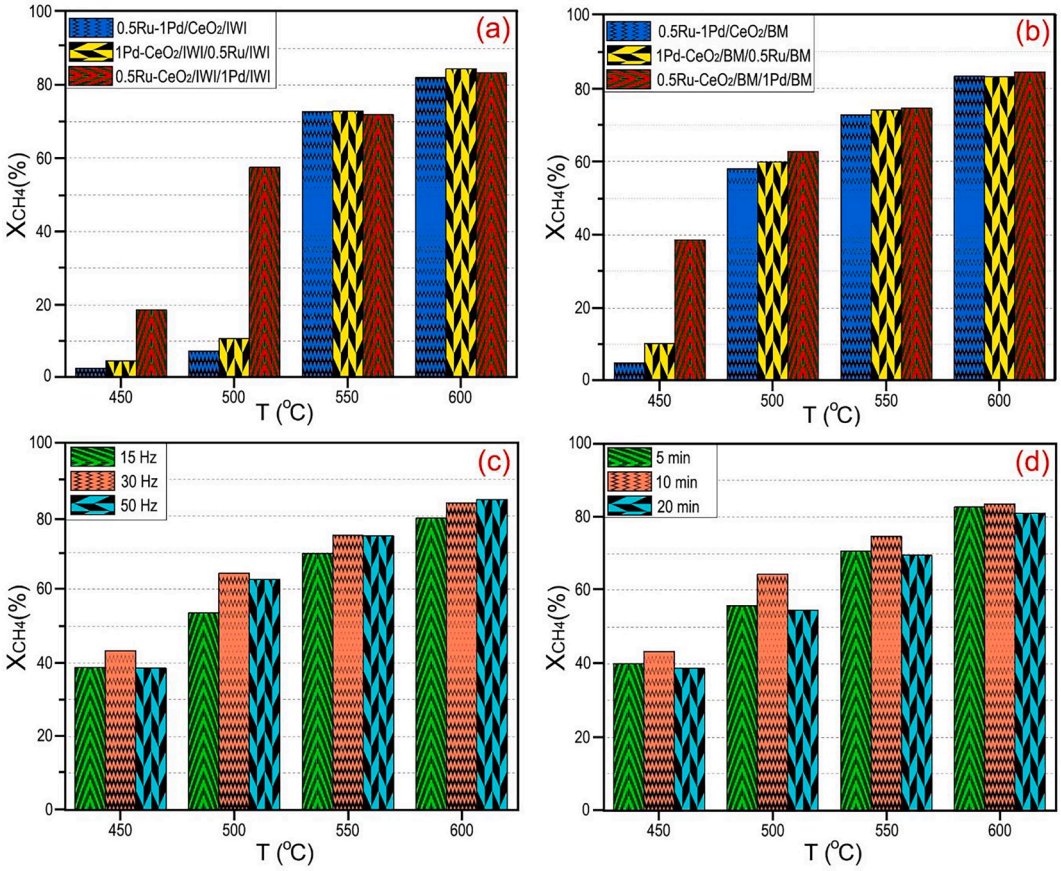

Fig. 5. Conversion of methane at 450–600 °C of bimetallic 0.5Ru–1Pd/CeO_2 catalysts prepared by co–impregnation and sequential impregnation (a) and one–step or two–steps ball milling at 50 Hz for 10 min (b). Conversion of methane at 450–600 °C of 0.5Ru–CeO_2/BM/1Pd/BM catalyst prepared with different milling frequencies (c) and different milling times (d). Reaction conditions: CH_4:air:N_2 = 4:11:85, F/W = 60 L h^{-1} g^{-1}, GHSV = 12 × 10^3h^{-1}.

the samples prepared by ball milling is always higher than the respective counterparts prepared by incipient wetness impregnation, and that these differences are particularly evident at low reaction temperature.

Fig. 5c and d show the conversion of methane of the 0.5Ru–CeO_2/BM/1Pd/BM catalyst prepared with different milling frequencies and different milling times, respectively, to infer the influence of the ball milling parameters on the catalytic activity (selectivity values and syngas yield are reported in Table 1). Both the milling frequency and time have a clear effect on the conversion of methane, particularly at low reaction temperature, which follows the order 30 Hz ~ 50 Hz > 15 Hz and 10 min > 5 min ~ 20 min. Therefore, a frequency of 30 Hz and 10 min milling time can be set as favorable synthesis conditions for the catalysts prepared by BM.

An important aspect regarding bimetallic catalysts is the relative amount of the two metals involved. In our case, it should be also considered that the cost of Pd is much higher than that of Ru, which has a direct impact on the final cost of the catalyst. Fig. 6a and 6b show the CH_4 conversion and syngas yield, respectively, at 450 °C and 600 °C for bimetallic Ru–CeO_2/BM/Pd/BM and Ru–CeO_2/IWI/Pd/IWI catalysts containing different amounts of Ru (from 0.06 to 1 wt%) and Pd (from

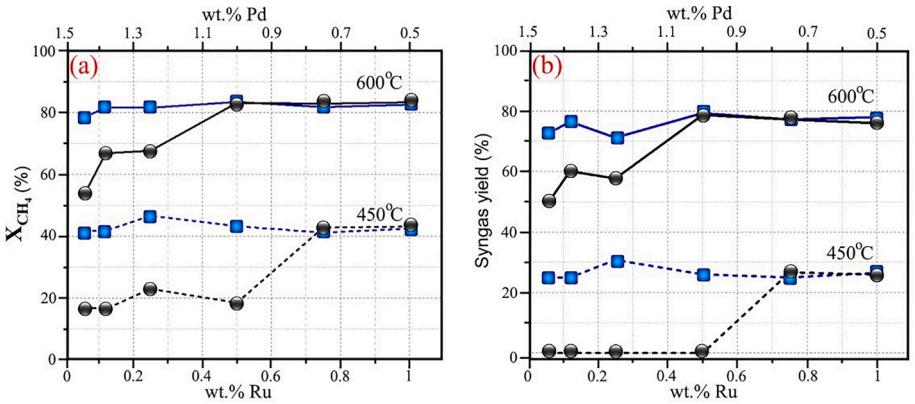

Fig. 6. Methane conversion (a) and syngas yield (b) at 450 °C and 600 °C for bimetallic catalysts xRu–yPd/CeO_2 prepared by two steps of BM (blue squares), and sequential-IWI (black circles) methods. All catalysts contain a nominal metal loading of 1.5 wt%. Reaction conditions: GHSV = 12 × 10^3h^{-1} and F/W = 60 L h^{-1} g^{-1}. Ball mill conditions: 30 Hz for 10 min. (For interpretation of the references to colour in this figure legend, the reader is referred to the web version of this article.)

0.5 to 1.44 wt%) and keeping the total metal loading at 1.5 wt%.

For the catalysts prepared by the IWI method there is a trend between the Ru content in the bimetallic samples and catalytic activity, being the catalysts with a progressive Ru loading more active in the transformation of methane and more selective to syngas. In sharp contrast, the samples prepared by the BM method do not follow this trend and no large differences in methane conversion and syngas selectivity are encountered, being methane conversion and syngas selectivity values much higher than those recorded on the catalysts prepared by the IWI method with the same composition, particularly at low temperature and low Ru content. It is important to note that the selectivity to syngas is maintained approximately constant at each temperature for the catalysts prepared by the BM method regardless of the relative metal content, whereas for the catalysts prepared by the IWI method the selectivity to syngas is strongly influenced by the relative amounts of the metals, being large quantities of Ru necessary to attain syngas selectivity values similar to those attained by the samples prepared by mechanochemistry. It should be highlighted that no syngas production was observed for temperatures lower than 550 °C for the Ru–CeO_2/BM (Table 1). Certainly, the bimetallic Ru–Pd system appears as a particularly appealing metal combination to conduct POM at low temperature, where very reactive and specific active sites are created by ball milling with ceria [52].

3.3. Characterization of catalysts after reaction

The Raman spectra recorded for the monometallic Ru and Pd samples and bimetallic Ru–Pd catalysts prepared by BM and IWI methods after the catalytic test discussed above are shown in Fig. 7. In all cases, the position of the F_{2g} band of CeO_2 did not shift after the catalytic test

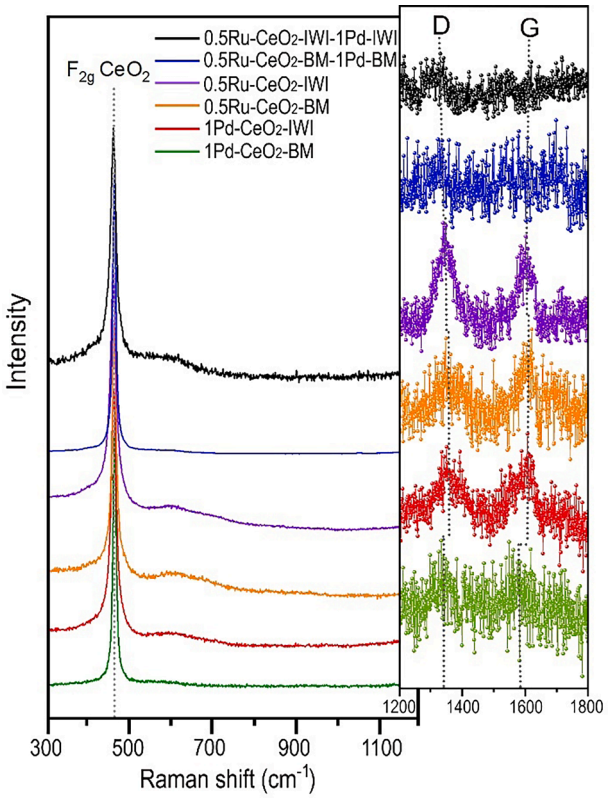

Fig. 7. Raman spectra of the monometallic catalysts 1Pd–CeO_2/BM, 1Pd–CeO_2/IWI, 0.5Ru–CeO_2/BM and0.5Ru–CeO_2/IWI, and bimetallic catalysts 0.5Ru–CeO_2/BM/1Pd/BM and 0.5Ru–CeO_2/IWI/1Pd/IWI after reaction at 600 °C. Reaction conditions: CH_4:air:N_2 = 4:11:85, F/W = 60 L h^{-1} g^{-1}, GHSV = 12 × $10^3 h^{-1}$. Ball milling conditions: 30 Hz for 10 min.

with respect to the values recorded before reaction (Fig. 1), suggesting that there is no incorporation of metals in the ceria structure during the reaction under the conditions tested. As expected, the B_{1g} mode of PdO and the symmetric ν_1 stretching mode of the nitrate anion in the monometallic Pd–CeO_2 prepared by both IWI and BM methods disappeared after reaction due to decomposition. In addition, the two characteristic graphite D and G bands at about ~ 1345 and ~ 1595 cm^{-1} [53,54] were observed in the Raman spectra of the catalysts after reaction. Even if their relative contribution in the spectra is certainly weak, it is possible to conclude that carbon deposition is more abundant in the monometallic samples and, in particular, on samples prepared by the IWI method. This constitutes another important issue, favoring the use of Ru–Pd/CeO_2 bimetallic catalysts prepared by ball milling.

Fig. 8 shows high–resolution transmission electron microscopy (HRTEM) images corresponding to monometallic Pd–CeO_2 and bimetallic Ru–Pd–CeO_2 catalysts prepared by both BM and IWI methods after reaction. Fig. 8a shows a representative image of the monometallic Pd–CeO_2 catalyst prepared by BM. The sample contains Pd nanoparticles, which measure about 3–4 nm and are well dispersed over the CeO_2 support (highlighted by green circles). The analysis of the lattice fringes by Fourier Transform (FT) images reveals the presence of spots at 1.94 Å from Pd^0 (200) planes and at 2.04 Å from PdO (101) crystallographic planes. Fig. 8b corresponds to the monometallic Pd–CeO_2 catalyst prepared by the IWI method. Again, both Pd^0 and PdO nanoparticles are identified, but their size is larger with respect to the Pd–CeO_2 catalyst prepared by BM, about 4–7 nm. Additionally, this catalyst shows the occurrence of carbon deposition, which is in accordance with the Raman results. Fig. 8c shows a representative image of the bimetallic Ru–CeO_2/BM/Pd/BM catalysts. However, it is difficult to distinguish any Ru, Pd or Ru–Pd particle in the HRTEM analysis, which indicates an excellent dispersion of Ru and Pd on the CeO_2 support. Additionally, the mechanochemical synthesis of the Ru–CeO_2/BM/Pd/BM catalyst creates an amorphous layer on the ceria crystallites, similar to that recently reported in Pd/CeO_2 catalysts prepared by BM [35], which is kept under reaction. This shell exhibits an average thickness of about 1–2 nm (marked between arrows). Fig. 8d corresponds to the bimetallic Ru–CeO_2/IWI/Pd/IWI catalyst. The HRTEM images for this sample show the presence of PdO and RuO_2 particles after reaction, with a size distribution of 4–7 nm.

The presence of reduced metal after reaction suggests that the catalysts are progressively reduced under reaction conditions due to the formation of syngas. Therefore, to get insight into the synergistic role played by Ru-Pd, we reduced the sample 0.5Ru-CeO_2/BM/1Pd/BM at 550 °C for 1 h before reaction (10 % H_2 in Ar, 20 mL min^{-1}). The results of methane conversion and syngas yield at different temperatures are shown in Fig. 9, which clearly shows that the reduction treatment is detrimental to the reaction. Therefore, it can be concluded that a direct reduction treatment is not beneficial for the synergistic effect between Ru and Pd in the ball milling samples, whereas the progressive reduction of the sample under reaction yields an optimum Ru-Pd interaction, being this effect particularly important at low reaction temperature.

3.4. Stability test

Bimetallic catalysts 0.5Ru–CeO_2/BM/1Pd/BM and 0.5Ru–CeO_2/IWI/1Pd/WI were tested for POM at 550 °C for>100 h to investigate stability issues. For comparative purposes, monometallic 0.5Ru–CeO_2/BM and 1Pd–CeO_2/BM samples were also tested. Fig. 10a and 10b show the methane conversion and syngas yield, respectively. As expected, the initial CH_4 conversion and syngas yield of the Ru–Pd/CeO_2 bimetallic catalysts were significantly higher than those of the monometallic samples, and the bimetallic catalyst prepared by the BM method performed better than the bimetallic counterpart prepared by the IWI method. Up to the first 50 h on stream, the catalytic performance of both Ru–Pd bimetallic catalysts prepared by either BM and IWI methods exhibited a constant decrease of the CH_4 conversion rate of ~ 0.03 %

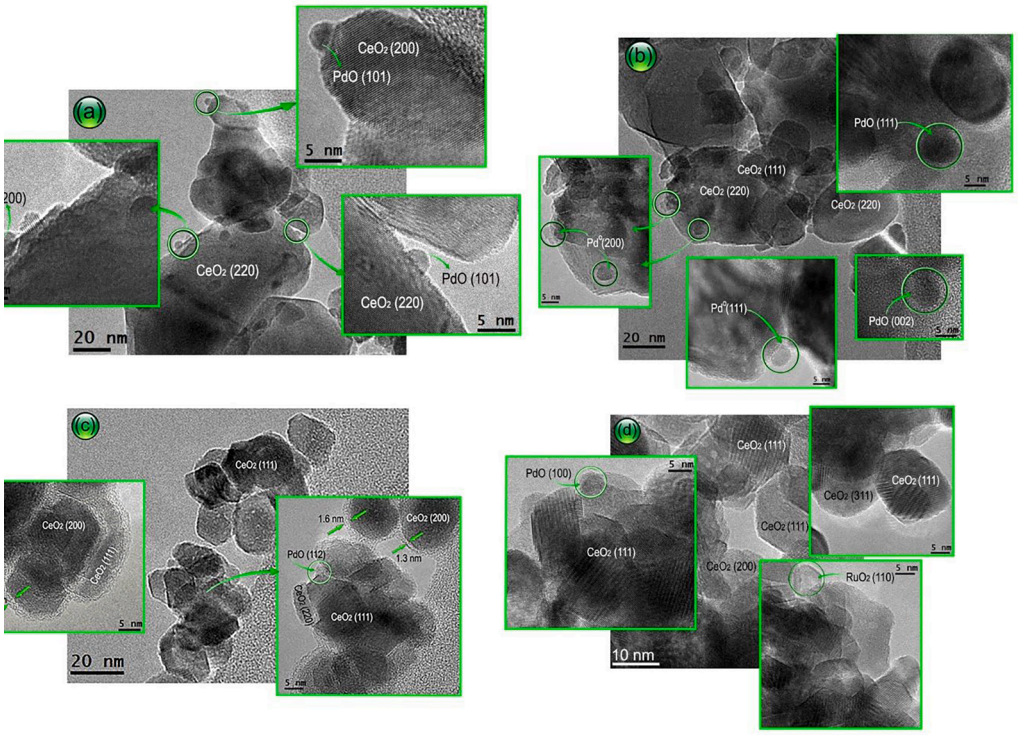

Fig. 8. HRTEM images of catalysts 1Pd–CeO_2/BM (a), 1Pd–CeO_2/IWI (b), 0.5Ru–CeO_2/BM/1Pd/BM (c) and 0.5Ru–CeO_2/IWI/1Pd/WI (d) after reaction at 600 °C. Reaction conditions: CH_4:air:N_2 = 4:11:85, F/W = 60 L h^{-1} g^{-1}, GHSV = 12 × $10^3 h^{-1}$. Ball milling conditions: 30 Hz for 10 min.

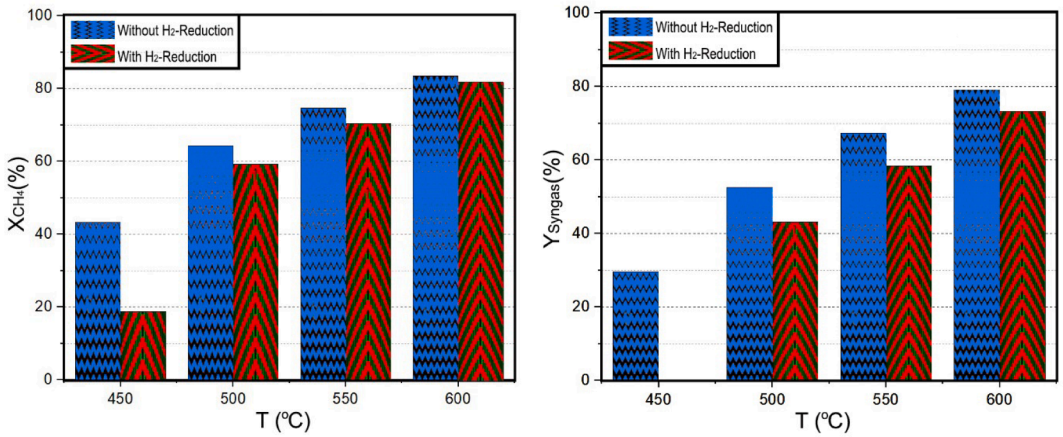

Fig. 9. Conversion of methane and yield of syngas on bimetallic catalyst 0.5Ru–CeO_2/BM/1Pd/BM reduced at 550 °C for 1 h. Reaction conditions: CH_4:air:N_2 = 4:11:85, F/W = 60 L h^{-1} g^{-1}, GHSV = 12 × $10^3 h^{-1}$. Ball milling conditions: 30 Hz for 10 min.

h^{-1}. On the other hand, the deactivation rate of methane conversion for the monometallic Ru–CeO_2/BM and Pd–CeO_2/BM were much higher, ~0.24 % h^{-1} and ~ 0.26 % h^{-1}, respectively. After 50 h on stream, the catalytic performance of the Ru–Pd bimetallic catalyst prepared by BM reached a steady–state in both CH_4 conversion and syngas yield, and the deactivation rate was practically zero (0.01 % h^{-1}). The methane conversion and syngas yield for this catalyst stabilized at ~ 70 % and ~ 60 %, respectively. In contrast, the performance of the Ru–Pd bimetallic catalyst prepared by the IWI method and the Ru and Pd monometallic samples did not stabilize and deactivation continued progressing, in particular for the 1Pd–CeO_2/BM sample. Under these reaction conditions, the catalysts' activity and stability follow the order: Ru–CeO_2/BM/Pd/BM > Ru–CeO_2/IWI/Pd/IWI > Ru/CeO_2/BM >> Pd–CeO_2/BM. Therefore, the bimetallic sample prepared by BM not only showed higher methane conversion and syngas production but also remarkably higher stability. On the other hand, it merits to be mentioned that, under exactly the same operation conditions, the catalytic stability of the Ru–Pd bimetallic catalyst prepared by the BM method is remarkably higher than that of the Ni–Pd bimetallic catalyst prepared by BM and with the same metal loading tested in our previous work [37].

Since the methane dry reforming is part of the POM reaction mechanism and commonly causes carbon deposition on the catalyst, Raman spectra were recorded on Pd–CeO_2/BM, Ru–CeO_2/BM/Pd/BM and Ru–CeO_2/IWI/Pd/IWI catalysts after the long–term stability test (Fig. 10c). The intensity of the D and G bands of carbon at about ~ 1410 and ~ 1650 cm^{-1}, respectively [35,39], follows the trend Pd–CeO_2/BM ≫ Ru–CeO_2/IWI/Pd/IWI > Ru–CeO_2/BM/Pd/BM, which is exactly the opposite trend of stability. Also, the quantification of carbon deposition by TGA yielded a remarkable higher value for Pd–CeO_2/BM (0.107 mg_C $g_{cat}^{-1} h^{-1}$) than for Ru–CeO_2/BM/Pd/BM (0.057 mg_C $g_{cat}^{-1} h^{-1}$)

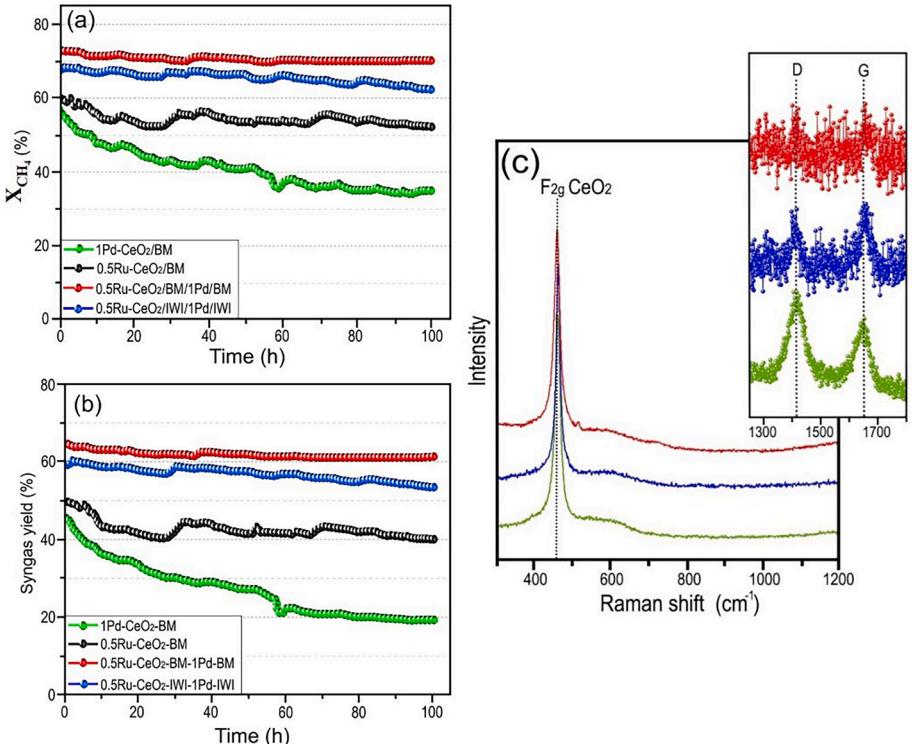

Fig. 10. Conversion of methane (a) and yield of syngas (b) in a long–term stability test at 550 °C on monometallic catalysts 1Pd–CeO_2/BM and 0.5Ru–CeO_2/BM, and bimetallic catalysts 0.5Ru–CeO_2/BM/1Pd/BM and 0.5Ru–CeO_2/IWI/1Pd/IWI. Raman spectra recorded on the samples after the long–term stability test (c). Reaction conditions: CH_4:air:N_2 = 4:11:85, F/W = 60 L h^{-1} g^{-1}, GHSV = 12 × $10^3 h^{-1}$. Ball milling conditions: 30 Hz for 10 min.

and Ru–CeO_2/IWI/Pd/IWI (0.059 mg_C $g_{cat}^{-1} h^{-1}$), even if carbon deposition can be considered low in all cases due to the lack of strong acid sites of the ceria support. Therefore, it can be concluded that the occurrence of carbon deposition can explain the deactivation observed for the catalysts during the stability test and that the low carbon deposition on the 0.5Ru–CeO_2/BM/1Pd/BM catalyst indicates its suitability to carry out POM under practical conditions.

4. Conclusions

In this study, CeO_2-supported monometallic Pd and Ru and bimetallic Pd-Ru catalysts have been prepared by ball milling and incipient wetness impregnation methods. The as-prepared catalysts have been characterized and tested for the POM reaction at atmospheric pressure to produce syngas between 300 and 600 °C. The catalytic results clearly demonstrated that the bimetallic Ru-Pd catalysts showed a greater activity and selectivity in comparison to monometallic Ru or Pd catalysts, and that the CH_4 conversion and syngas yield observed for different catalysts followed the order: Ru-CeO_2/BM/Pd/BM ≥ Ru-CeO_2/IWI/Pd/IWI ≫ Ru-CeO_2/BM ~ Pd-CeO_2/IWI ≥ Ru-CeO_2/IWI ~ Pd-CeO_2/BM ≫ CeO_2. The results suggest a strong synergy between Ru and Pd on CeO_2 occurring in the bimetallic samples prepared by sequential-BM, resulting in much more active sites for POM, particularly at temperatures below 500 °C. Therefore, we are currently performing further accurate operando characterization, such as XRD, X-ray absorption spectroscopy and ambient pressure-XPS using synchrotron light the elucidate the precise nature of the metal-support interaction of the Ru-Pd bimetallic catalysts prepared by mechanochemical method. Additionally, the bimetallic Ru-Pd catalysts prepared by two steps of BM not only produced syngas at a lower temperature, but also showed excellent stability in long-term experiments during 100 h on stream at 550 °C, with no coke deposited on it, outperforming by a large extent those of the bimetallic Ru-Pd catalysts prepared by sequential-IWI, and the monometallic Ru-CeO_2 and Pd-CeO_2 catalysts. Moreover, by studying the effect of Ru and Pd loadings in the bimetallic Ru-CeO_2/BM-IWI/Pd/BM-IWI catalysts prepared by sequential-IWI and two steps of BM, it has been proved that whereas the methane conversion increased gradually with the Ru content for the Ru-CeO_2/IWI/Pd/IWI catalysts, it was maintained approximately constant for the Ru-CeO_2/BM/Pd/BM samples. The best catalytic performance with maximum methane conversion and syngas yield values was obtained with catalysts containing 0.25 wt% Ru and 1.25 wt% Pd (0.25PRu- CeO_2/BM/1.25Pd/BM). Given the obtained results, highly active catalysts for POM can be designed and prepared by ball milling, a simple and scalable method, by using small amounts of Pd and Ru.

CRediT authorship contribution statement

Shiva Fazlikeshteli: Investigation, Formal analysis, Data curation, Writing – original draft, Visualization. **Xavier Vendrell:** Conceptualization, Methodology, Validation, Writing – review & editing, Visualization, Supervision. **Jordi Llorca:** Conceptualization, Methodology, Validation, Writing – review & editing, Visualization, Supervision, Project administration, Funding acquisition.

Declaration of Competing Interest

The authors declare the following financial interests/personal relationships which may be considered as potential competing interests: Jordi Llorca reports financial support was provided by Spain Ministry of Science and Innovation. Jordi Llorca reports financial support was provided by Government of Catalonia. Xavier Vendrell reports financial support was provided by Ministerio de Ciencia, Innovación y Universidades. Shiva Fazlikeshteli reports financial support was provided by Government of Catalonia.

Data availability

Data will be made available on request.

Acknowledgments

This research was funded by MICINN/FEDER PID2021-124572OB-C31 and 2017 SGR 128 grants. S.F. is grateful to Generalitat de Catalunya for PhD grant 2019 FI_B 00908. XV is grateful to Spanish Government, Ministerio de Ciencia, Innovación y Universidades Juan de la Cierva-Incorporación program for an individual fellowship grant agreement IJCI-2017-31449. J.L. is a Serra Húnter Fellow and is grateful to the ICREA Academia program.

References

[1] Dedov A, et al. High-selectivity partial oxidation of methane into synthesis gas: the role of the red-ox transformations of rare earth—alkali earth cobaltate-based catalyst components. Fuel Process Technol 2016;148:128–37.
[2] Freni S, Calogero G, Cavallaro S. Hydrogen production from methane through catalytic partial oxidation reactions. J Power Sources 2000;87(1–2):28–38.
[3] Fakeeha AH, Al-Fatesh AS, Abasaeed AE. Modification of alumina support with TiO2-P25 in CO2 reforming of CH4. J Ind Eng Chem 2012;18(1):212–7.
[4] Moral A, et al. Partial oxidation of methane to syngas using Co/Mg and Co/Mg-Al oxide supported catalysts. Catal Today 2019;333:259–67.
[5] Makarshin L, et al. Catalytic partial oxidation of methane in microchannel reactors with co-current and countercurrent reagent flows: An experimental comparison. Chem Eng J 2011;178:276–81.
[6] Xie J, et al. Autothermal reforming and partial oxidation of n-hexadecane via Pt/Ni bimetallic catalysts on ceria-based supports. Int J Hydrogen Energy 2015;40(27):8510–21.
[7] Khajenoori M, Rezaei M, Nematollahi B. Preparation of noble metal nanocatalysts and their applications in catalytic partial oxidation of methane. J Ind Eng Chem 2013;19(3):981–6.
[8] Maniecki TP, et al. Effect of the chemical composition of (MgO) x (Al2O3) y support on the catalytic performance of Ni and Ni–Au catalysts for the partial oxidation of methane. Chem Eng J 2009;154(1–3):142–8.
[9] Navarro RM, Pena M, Fierro J. Hydrogen production reactions from carbon feedstocks: fossil fuels and biomass. Chem Rev 2007;107(10):3952–91.
[10] Kriz DA, et al. Partial Oxidation of Methane to Synthesis Gas Using Supported Ga-Containing Bimetallic Catalysts and a Ti-Promoter. ChemCatChem 2018;10(19):4300–8.
[11] Requies J, et al. Nickel/alumina catalysts modified by basic oxides for the production of synthesis gas by methane partial oxidation. Catal Today 2006;116(3):304–12.
[12] Cifuentes B, et al. Monoliths washcoated with AuCu catalysts for CO removal in an ethanol fuel processor: Effect of CeO2–SiO2 dual support on the catalytic performance and reactor cost. Int J Hydrogen Energy 2021;46(2):2166–81.
[13] Ashcroft A, et al. Selective oxidation of methane to synthesis gas using transition metal catalysts. Nature 1990;344(6264):319–21.
[14] Tsang S, Claridge J, Green M. Recent advances in the conversion of methane to synthesis gas. Catal Today 1995;23(1):3–15.
[15] Hickman D, Haupfear E, Schmidt L. Synthesis gas formation by direct oxidation of methane over Rh monoliths. Catal Lett 1993;17(3):223–37.
[16] Hickman D, Schmidt L. Production of syngas by direct catalytic oxidation of methane. Science 1993;259(5093):343–6.
[17] Hickman D, Schmidt LD. Steps in CH4 oxidation on Pt and Rh surfaces: High-temperature reactor simulations. AIChE J 1993;39(7):1164–77.
[18] Poirier MG, Trudel J, Guay D. Partial oxidation of methane over ruthenium catalysts. Catal Lett 1993;21(1):99–111.
[19] Horn R, et al. Methane catalytic partial oxidation on autothermal Rh and Pt foam catalysts: Oxidation and reforming zones, transport effects, and approach to thermodynamic equilibrium. J Catal 2007;249(2):380–93.
[20] Yamagishi T, et al. Catalytic performance and characterization of RhVO4/SiO2 for hydroformylation and CO hydrogenation. J Mol Catal A: Chem 2006;244(1–2):201–12.
[21] Tomishige K, Asadullah M, Kunimori K. Syngas production by biomass gasification using Rh/CeO2/SiO2 catalysts and fluidized bed reactor. Catal Today 2004;89(4):389–403.
[22] Torniainen P, Chu X, Schmidt L. Comparison of monolith-supported metals for the direct oxidation of methane to syngas. J Catal 1994;146(1):1–10.
[23] Chen W, et al. Titanium-promoted Rh-Mn-Li/SiO2 for C2-oxygenates synthesis from syngas: effect of low titanium loading. J Nat Gas Chem 2005;14(4):199–206.
[24] Choudhary VR, Mondal KC, Mulla SA. Simultaneous conversion of methane and methanol into gasoline over bifunctional Ga-, Zn-, In-, and/or Mo-modified ZSM-5 zeolites. Angew Chem 2005;117(28):4455–9.
[25] Kaila RK, et al. Zirconia-supported bimetallic RhPt catalysts: Characterization and testing in autothermal reforming of simulated gasoline. Appl Catal B 2008;84(1–2):223–32.
[26] Nikolla E, Schwank J, Linic S. Promotion of the long-term stability of reforming Ni catalysts by surface alloying. J Catal 2007;250(1):85–93.
[27] Zhang J, Wang H, Dalai AK. Development of stable bimetallic catalysts for carbon dioxide reforming of methane. J Catal 2007;249(2):300–10.
[28] Luo Z, et al. TiO2 Supported gold–palladium catalyst for effective syngas production from methane partial oxidation. Appl Catal A 2018;554:54–63.
[29] Ramírez-López R, Elizalde-Martinez I, Balderas-Tapia L. Complete catalytic oxidation of methane over Pd/CeO2–Al2O3: The influence of different ceria loading. Catal Today 2010;150(3–4):358–62.
[30] Wang Y, Zhang J. Hydrogen production on Ni–Pd–Ce/γ-Al2O3 catalyst by partial oxidation and steam reforming of hydrocarbons for potential application in fuel cells. Fuel 2005;84(14–15):1926–32.
[31] Mustu, H., et al., *Effect of synthesis route of mesoporous zirconia based Ni catalysts on coke minimization in conversion of biogas to synthesis gas.* international journal of hydrogen energy, 2015. **40**(8): p. 3217-3228.
[32] da Silva AM, et al. Study of the performance of Rh/La2O3–SiO2 and Rh/CeO2 catalysts for SR of ethanol in a conventional fixed-bed reactor and a membrane reactor. International Journal of Hydrogen Energy 2015;40(11):4154–66.
[33] Wang, Z., et al., *Self-sustained electrochemical promotion catalysts for partial oxidation reforming of heavy hydrocarbons.* international journal of hydrogen energy, 2012. **37**(23): p. 17928-17935.
[34] Xu X, Li P, Shen Y. Small-scale reforming of diesel and jet fuels to make hydrogen and syngas for fuel cells: A review. Appl Energy 2013;108:202–17.
[35] Fazlikeshteli S, Vendrell X, Llorca J. Low-Temperature Methane Partial Oxidation over Pd Supported on CeO2: Effect of the Preparation Method and Precursors. Reactions 2021;2(1):30–42.
[36] Danielis M, Colussi S, de leitenburg, C., Soler, L., Llorca, J., Trovarelli, A.. Outstanding Methane Oxidation Performance of Pd-Embedded Ceria Catalysts Prepared by a One-step Dry Ball-Milling Method. Angew Chem 2018;130:10369–73.
[37] Fazlikeshteli S, Vendrell X, Llorca J. Low-temperature partial oxidation of methane over Pd–Ni bimetallic catalysts supported on CeO2. Int J Hydrogen Energy 2022.
[38] Engineering, D.o.C.a.B. *Bioanalytical Microfluidics Program.* 2019; Available from: http://cbe.colostate.edu/.
[39] Wu Z, et al. Probing defect sites on CeO2 nanocrystals with well-defined surface planes by Raman spectroscopy and O2 adsorption. Langmuir 2010;26(21):16595–606.
[40] Weber W, Hass K, McBride J. Raman study of CeO2: Second-order scattering, lattice dynamics, and particle-size effects. Physical Review B 1993;48(1):178.
[41] Ma J, et al. The relationship between the chemical state of Pd species and the catalytic activity for methane combustion on Pd/CeO2. Catal Sci Technol 2018;8(10):2567–77.
[42] Lucentini I, et al. Ammonia decomposition over 3D-printed CeO2 structures loaded with Ni. Appl Catal A 2020;591:117382.
[43] Lucentini I, et al. Catalytic ammonia decomposition over Ni-Ru supported on CeO2 for hydrogen production: Effect of metal loading and kinetic analysis. Appl Catal B 2021;286:119896.
[44] Zhang J, et al. Performance of bimetallic PdRu catalysts supported on gamma alumina for 2-ethylanthraquinone hydrogenation. RSC Adv 2017;7(11):6447–56.
[45] Zhu H, et al. Pd/CeO2–TiO2 catalyst for CO oxidation at low temperature: a TPR study with H2 and CO as reducing agents. J Catal 2004;225(2):267–77.
[46] Pérez-Bustos HF, et al. Synthesis and characterization of bimetallic catalysts Pd-Ru and Pt-Ru supported on γ-alumina and zeolite FAU for the catalytic transformation of HMF. Fuel 2019;239:191–201.
[47] Pang J, et al. Mesoporous Cu2O–CeO2 composite nanospheres with enhanced catalytic activity for 4-nitrophenol reduction. Appl Surf Sci 2018;439:420–9.
[48] Ho P, et al. One-step electrodeposition of Pd–CeO2 on high pore density foams for environmental catalytic processes. Catal Sci Technol 2018;8(18):4678–89.
[49] Danielis M, et al. Methane oxidation activity and nanoscale characterization of Pd/CeO2 catalysts prepared by dry milling Pd acetate and ceria. Appl Catal B 2022;282:119567.
[50] Enger BC, Lødeng R, Holmen A. A review of catalytic partial oxidation of methane to synthesis gas with emphasis on reaction mechanisms over transition metal catalysts. Appl Catal A 2008;346(1–2):1–27.
[51] York AP, Xiao T, Green ML. Brief overview of the partial oxidation of methane to synthesis gas. Top Catal 2003;22(3–4):345–58.
[52] Hannemann S, et al. Combination of flame synthesis and high-throughput experimentation: The preparation of alumina-supported noble metal particles and their application in the partial oxidation of methane. Appl Catal A 2007;316(2):226–39.
[53] Han Z, et al. Propane dehydrogenation over Pt–Cu bimetallic catalysts: the nature of coke deposition and the role of copper. Nanoscale 2014;6(17):10000–8.
[54] Chen Y, Chen J. Selective hydrogenation of acetylene on SiO2 supported Ni-In bimetallic catalysts: Promotional effect of In. Appl Surf Sci 2016;387:16–27.